Observer-Based Sensor Fusion for Power-Assist Electric Bicycles

Chun-Feng Huang, Bang-Hao Dai, and T.-J. Yeh*

Abstract— **In this paper, a sensor fusion algorithm is proposed for electric bicycles to accomplish power-assist function without using torque sensors. The sensor fusion is observer-based and uses outputs from the wheel encoder and a 6-axis inertial measurement unit to estimate the longitudinal acceleration of the bicycle and the slope angle of the road. It is mainly based on the kinematic model that describes the time-varying characteristics of the gravity vector in a moving frame. By exploiting the structure of the observer model, convergence of the estimation errors can be easily achieved by selecting two sub-gain matrices in spite of the time-varying characteristics of the model. The fusion results allow one to conduct mass compensation, gravity compensation and friction compensation for power-assist purposes. With the compensations, riding the power-assist bike on hills is similar to riding a conventional bicycle on the level ground regardless the weight increase by the battery and the motor.**

I. Introduction

As the first kind of personal mobility vehicles ever invented, bicycles play an important role in the history of transport. Bicycles are lightweight and are powered by human. They can contribute to the reduction of traffic congestion and air pollution in urban areas. With the advances in motor and control technologies, electric bicycles (also known as E-bikes) were introduced to further enhance the mobility of bicycles. Among the various E-bikes in the market, power-assist E-bikes retain the ability to be pedaled by the rider and can generate appropriate motor torque to assist rider's pedaling. They make hill-climbing easier and can extend the range of travel without exhausting the rider.

In most power-assist E-bikes, the rider's pedaling torque is measured by the torque sensor and then amplified by the motor. However, torque sensors are usually bulky, expensive, and can not be directly mounted without modifying the bicycle structure[1]. Therefore, several alternative methods have been proposed to replace torque sensors to estimate the pedaling torque. For instance, Kurosawa, et. al.[2] used a disturbance observer together with the control input torque and the vehicle acceleration to estimate the external torque acting on the bicycle. Then the pedal torque is extracted from the estimated external torque using Fourier transform by considering that the pedaling torque has twice frequency of pedaling periods. However, the acceleration signal used therein is obtained by differentiating the wheel speed measured by the encoder; thus is susceptible to computation delays and numerical noises. A similar approach is adopted in [3] except that the acceleration is directly picked up by an accelerometer and the pedaling torque is computed by an iterative least square method instead. Since the maneuvering of the bicycle is three-dimensional, in addition to the acceleration in the longitudinal direction, the accelerometer also picks up centrifugal and/or gravitational acceleration; thus could lead to an erroneous estimation of the pedaling torque.

While replacing torque sensors by wheel encoders or accelerometers alone does not produce acceptable estimation for the pedaling torque, this study is devoted to using multi-sensor fusion to seek other crucial information to achieve power-assist function in E-bikes. Sensor fusion has been widely used in aeronautics and astronautics to determine the attitudes of an aircraft or a spacecraft[4][5]. The fusion combines measurement data from accelerometers and gyros in an inertial measurement unit (IMU) and other sensors by methods such as extended Kalman filter, complementary filter and so on. Sensor fusion has also been applied in vehicle research to enhance the performance of stability and traction control systems. In these cases, the IMU's are fused with GPS sensors to estimate vehicle states such as side-slip angle, roll angle and so on[6][7].

In this paper, sensor fusion is performed on the outputs from the wheel encoder and a 6-D IMU which contains a three-axis accelerometer and a three-axis rate gyro. The fusion results allow one to conduct mass compensation, gravity compensation and friction compensation for power-assist purposes. With the compensations, riding the power-assist bike on hills will be similar to riding a conventional bicycle on the level ground regardless of the weight increase by the battery and the motor. The paper is organized as follows: The principle of power assist is given in section II. Section III presents a model that characterizes the kinematics of the measured signals. Using this model, an observer is constructed in section IV to estimate the states needed for power assist. The performance of the sensor fusion algorithm and the power-assist function is validated experimentally in section V. Finally, conclusions are given in section VI .

II. Principle of Power Assist

According to the schematic in Fig. 1, the dynamics of an E-bike in the longitudinal direction is governed by the equation of motion:

$$Ma = F_p - F_f - Mg\sin\psi + F_m, \tag{1}$$

where M represents the total mass of the bicycle plus the rider, g is the gravitational acceleration, a and ψ are respectively the longitudinal acceleration and the slope of

All authors are with Department of Power Mechanical Engineering, National Tsing Hua University, Hsinchu 30013, Taiwan. benson516@hotmail.com; spring9527@gmail.com; tyeh@pme.nthu.edu.tw

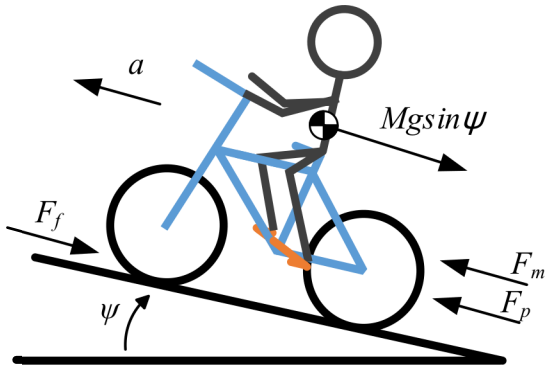

Fig. 1. Schematic of an E-bike in the sagittal plane

the road, F_p is the propulsion force generated by rider's pedaling, F_f is the friction force, and F_m is the propulsion force provided by the motor. The power-assist function uses F_m to perform compensation on the system dynamics. In this study, F_m takes the form:

$$F_m = \eta M a + M g \sin\psi + F_f, \tag{2}$$

where $0 < \eta < 1$ is the assistive ratio.

In (2), the compensation consists of three terms: mass compensation, gravity compensation, and friction compensation. These compensations are mutually independent and can be designed separately.

1) Mass compensation: Mass compensation uses the longitudinal acceleration (a) to generate the compensation force. The equivalent total mass seen from the rider (F_p) is reduced to $(1-\eta)M$. This implies that the rider has better control on the acceleration or deceleration of the bicycle. Theoretically, η which is the ratio of mass compensation, can be any value between 0 and 1 depending on the amount of compensation needed. However, for stability consideration, the compensated mass should not exceed the mass of the bicycle m_b, *i.e.* $0 \le \eta < \frac{m_b}{M}$. The discussion about the constraint on η is given in the appendix.
2) Gravity compensation: The gravity compensation uses the slope angle (ψ) to generate the compensation force $Mg\sin\psi$ to cancel the gravity force acting on the bicycle. This implies that during uphill climbing the rider has the same feeling as travelling on the level ground, and regenerative braking is automatically applied on the bicycle when travelling downhill.
3) Friction compensation: The friction compensation is meant to compensate for the major friction force acting on the bicycle, the rolling friction. Rolling friction is proportional to the normal force on the tire, or is given by:

$$F_f = f_r M g \cos\psi,$$

in which f_r is the rolling friction coefficient.

III. Kinematic Modeling

The power-assist function in discussion requires measurements on the slope angle of the road and the acceleration of the bicycle. The accelerometers can sense these two quantities simultaneously but are not able to separate them without incorporating data from rate gyros and/or other sensors. What makes the separation of the angle and the acceleration information more intriguing is that sensors mounted on bicycles not only experience pitch, roll, and yaw motion all together but are also subjected to both inertia and centrifugal forces. In this paper, an observer-based sensor fusion algorithm is proposed to obtain reliable information for power assist using the accelerometer and rate gyro signals from an IMU and the velocity signal from a wheel encoder. The observer design is based on the kinematic model discussed below.

The discussion starts with defining the coordinate frames. An IMU senor frame $X_sY_sZ_s$ is fixed to the bicycle so that the Z_s axis is in the longitudinal direction and the Y_s axis is perpendicular to the bicycle plane. The orientation of the inertia frame $X_IY_IZ_I$ with respect to the sensor frame is defined by three elementary rotations. According to Fig. 2, the $X_IY_IZ_I$ frame is firstly rotated by a yaw angle ϕ about the X_I axis to arrive at an intermediate frame $X'Y'Z'$. Then the $X'Y'Z'$ frame is rotated by a pitch angle ψ about the Y' axis to arrive at another intermediate frame $X"Y"Z"$. Finally, $X_s\,Y_sZ_s$ is obtained by rotating the $X"Y"Z"$ frame about the $Z"$ axis by a roll angle θ.

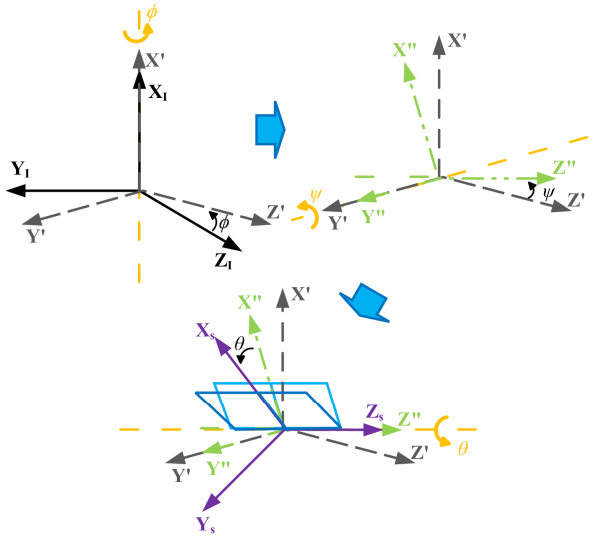

Fig. 2. Coordinate definitions of Euler angles

The rotation matrix $\mathbf{R}_i^s$ that defines the coordination transformation from the $X_IY_IZ_I$ frame to the $X_sY_sZ_s$ frame can thus be expressed as multiplication of three matrices of elementary rotation, i.e.

$$\begin{aligned}\mathbf{R}_i^s &= \mathbf{R}(\theta)\mathbf{R}(\psi)\mathbf{R}(\phi)\\ &= \begin{bmatrix} c_\theta c_\psi & c_\theta s_\phi s_\psi + c_\phi s_\theta & -c_\phi c_\theta s_\psi + s_\phi s_\theta \\ -s_\theta c_\psi & -s_\phi s_\psi s_\theta + c_\phi c_\theta & c_\phi s_\psi s_\theta + c_\theta s_\phi \\ s_\psi & -c_\psi s_\phi & c_\psi c_\phi \end{bmatrix}\end{aligned}$$

where $\mathbf{R}(\psi) = \begin{bmatrix} c_\psi & 0 & -s_\psi \\ 0 & 1 & 0 \\ s_\psi & 0 & c_\psi \end{bmatrix}$,

$\mathbf{R}(\theta) = \begin{bmatrix} c_\theta & s_\theta & 0 \\ -s_\theta & c_\theta & 0 \\ 0 & 0 & 1 \end{bmatrix}$, and $\mathbf{R}(\phi) = \begin{bmatrix} 1 & 0 & 0 \\ 0 & c_\phi & s_\phi \\ 0 & -s_\phi & c_\phi \end{bmatrix}$.

Note that the notations $c_{(\cdot)}$ and $s_{(\cdot)}$ are the abbreviations for $\cos(\cdot)$ and $\sin(\cdot)$, respectively; such short-hand notations will be adopted throughout the paper.

The three-axis rate gyro in the IMU measures the absolute angular velocity in the $X_sY_sZ_s$ coordinates. The vectorial form of the gyro measurements, denoted by $\boldsymbol{\omega}$, can be computed by

$$\begin{aligned} \boldsymbol{\omega} &= \mathbf{R}(\theta)\mathbf{R}(\psi)\begin{bmatrix} \dot\phi \\ 0 \\ 0 \end{bmatrix} + \mathbf{R}(\theta)\begin{bmatrix} 0 \\ \dot\psi \\ 0 \end{bmatrix} + \begin{bmatrix} 0 \\ 0 \\ \dot\theta \end{bmatrix} \quad (3) \\ &= \begin{bmatrix} \dot\phi c_\theta c_\psi + \dot\psi s_\theta \\ -\dot\phi s_\theta c_\psi + \dot\psi c_\theta \\ \dot\phi s_\psi + \dot\theta \end{bmatrix}. \end{aligned}$$

The three-axis accelerometer in the IMU measures the acceleration in the $X_sY_sZ_s$ frame. The sensor frame is a non-inertial frame, so the measured acceleration consists of the gravity, the inertia acceleration (which equals $-a$) and the centrifugal acceleration. Particularly, the gravity vector in the the $X_sY_sZ_s$ frame, is denoted by $\mathbf{g}_s$ and is given by

$$\mathbf{g}_s = \mathbf{R}_i^s \begin{bmatrix} -g \\ 0 \\ 0 \end{bmatrix} = \begin{bmatrix} -gc_\theta c_\psi \\ gs_\theta c_\psi \\ -gs_\psi \end{bmatrix},$$

where $g = 9.8m/s^2$. Considering that gravity in the $X_IY_IZ_I$ frame is a fixed vector and the sensor frame rotates with an angular velocity of $\boldsymbol{\omega}$, the kinematic model that describes the time-varying characteristics of $\mathbf{g}_s$ can be derived as $\dot{\mathbf{g}}_s = -\boldsymbol{\omega} \times \mathbf{g}_s$ or, in the state-space form,

$$\dot{\mathbf{g}}_s = \boldsymbol{\Omega}\mathbf{g}_s, \quad (4)$$

where $\boldsymbol{\Omega} = \begin{bmatrix} 0 & \omega_3 & -\omega_2 \\ -\omega_3 & 0 & \omega_1 \\ \omega_2 & -\omega_1 & 0 \end{bmatrix}$ with ω_i being the ith component of $\boldsymbol{\omega}$. Because the sensor frame is non-inertial, other than gravity, the accelerometer also measures the inertia acceleration (which equals $-a$) and the centrifugal acceleration. With Z_s axis in the longitudinal direction and Y_s axis perpendicular to the bicycle plane, the output of the three-axis accelerometer, which is denoted by $\mathbf{a}_s$, can be written as:

$$\mathbf{a}_s = \mathbf{g}_s + \begin{bmatrix} a_{cx} \\ a_{cy} \\ -a + a_{cz} \end{bmatrix}. \quad (5)$$

with a_{cx}, a_{cy}, and a_{cz} being components of the centrifugal acceleration along the three sensor axes.

Both the state equation (4) and the output equation (5) are linear. Viewing a and $a_{c(.)}$ as the sensor noises, it is possible to construct an observer to estimate $\mathbf{g}_s$. Then performing trigonometric algebra on the components of $\mathbf{g}_s$, one can compute the roll angle θ and the pitch angle ψ. Before proceeding to the observer design, it should be noted that the filtering nature of the observer makes it less immune to the low-frequency contents of a and $a_{c(.)}$. Therefore, in order to get an accurate estimate for $\mathbf{g}_s$, at least the low-frequency contents of a and $a_{c(.)}$ need to be characterized.

The low-frequency content of a, which is denoted by a_{lpf}, is assumed to a low-pass filtering version of a by the first-order differential equation:

$$\dot a_{lpf} = -\alpha \cdot a_{lpf} + \alpha \cdot a. \quad (6)$$

where α is the filter bandwidth. Examining the third row in (5), the acceleration a is equal to $g_{s3} - a_{s3} + a_{cz}$ where g_{s3} and a_{s3} are the third components of $\mathbf{g}_s$ and $\mathbf{a}_s$ respectively. Substituting such a relation into (6) leads to

$$\dot a_{lpf} = -\alpha \cdot a_{lpf} + \alpha \cdot g_{s3} - \alpha \cdot a_{s3} + \alpha \cdot a_{cz}. \quad (7)$$

The velocity computed from the output of wheel encoder is used to estimate a_{lpf}. The time derivative of the velocity v is equal to the acceleration, so

$$\dot v = a = g_{s3} - a_{s3} + a_{cz}. \quad (8)$$

Define the state vector as $\mathbf{x} = \begin{bmatrix} \mathbf{g}_s \\ a_{lpf} \\ v \end{bmatrix}$. The state equation for observer design is obtained by combining (4), (7), and (8). It is given by

$$\dot{\mathbf{x}} = \mathbf{A}\mathbf{x} + \mathbf{u}, \quad (9)$$

where $\mathbf{A} = \begin{bmatrix} \boldsymbol{\Omega} & & \mathbf{0}_{3\times 2} \\ 0 & 0 & \alpha & -\alpha & 0 \\ 0 & 0 & 1 & 0 & 0 \end{bmatrix}$ and $\mathbf{u} = \begin{bmatrix} \mathbf{0}_{3\times 1} \\ -\alpha \cdot a_{s3} + \alpha \cdot a_{cz} \\ -a_{s3} + a_{cz} \end{bmatrix}$. Notice that the system is linear but time varying due to the presence of $\boldsymbol{\Omega}$ in $\mathbf{A}$. On the other hand, the accelerometer output $\mathbf{a}_s$ and the velocity signal v constitute the output vector $\mathbf{y}$. The output equation thus is given by

$$\mathbf{y} = \begin{bmatrix} \mathbf{a}_s \\ v \end{bmatrix} = \begin{bmatrix} \mathbf{g}_s \\ v \end{bmatrix} + \begin{bmatrix} a_{cx} \\ a_{cy} \\ -a + a_{cz} \\ 0 \end{bmatrix}.$$

Considering that the acceleration a can be written as $a = a_{lpf} + a_{hpf}$, where a_{lpf} is one of the state variables and a_{hpf} is the high-frequency content of a, one can express $\mathbf{y}$ in the standard state-space form as

$$\mathbf{y} = \mathbf{C}\mathbf{x} + \mathbf{v}, \quad (10)$$

where $\mathbf{C} = \begin{bmatrix} \mathbf{I}_{3\times 3} & \mathbf{0}_{2\times 2} \\ \mathbf{0}_{1\times 3} & -1 \quad 0 \\ & 0 \quad 1 \end{bmatrix}$ and $\mathbf{v} = \begin{bmatrix} a_{cx} \\ a_{cy} \\ -a_{hpf} + a_{cz} \\ 0 \end{bmatrix}$.

IV. Observer Design

Based on (9) and (10), the observer that produces the estimated state vector $\hat{\mathbf{x}}$ is proposed as follows:

$$\dot{\hat{\mathbf{x}}} = \mathbf{A}\hat{\mathbf{x}} + \hat{\mathbf{u}} + \mathbf{L}(\mathbf{C}\hat{\mathbf{x}} + \hat{\mathbf{v}} - \mathbf{y}), \tag{11}$$

where $\mathbf{L}$ is the observer gain matrix, $\hat{\mathbf{u}}$ and $\hat{\mathbf{v}}$ are respectively the estimation for $\mathbf{u}$ and $\mathbf{v}$. The error dynamics is thus given by subtracting (9) from (11)

$$\dot{\tilde{\mathbf{x}}} = (\mathbf{A} + \mathbf{LC})\,\tilde{\mathbf{x}} + \mathbf{L}\tilde{\mathbf{v}} + \tilde{\mathbf{u}}, \tag{12}$$

where $\tilde{\mathbf{x}} = \hat{\mathbf{x}} - \mathbf{x}$, $\tilde{\mathbf{v}} = \hat{\mathbf{v}} - \mathbf{v}$ and $\tilde{\mathbf{u}} = \hat{\mathbf{u}} - \mathbf{u}$.

While the expressions for $\hat{\mathbf{u}}$ and $\hat{\mathbf{v}}$ will be given later, the $\mathbf{L}$ is designed as

$$\mathbf{L} = \mathbf{L}_{\mathbf{\Omega}} + \bar{\mathbf{L}}, \tag{13}$$

where $\mathbf{L}_\Omega = \begin{bmatrix} -\mathbf{\Omega} & \mathbf{0}_{3\times1} \\ \mathbf{0}_{2\times3} & \mathbf{0}_{2\times1} \end{bmatrix}$ is used to cancel most of the time-varying content in $\mathbf{A}$, and $\bar{\mathbf{L}}$ is a constant matrix for placing the observer poles. Substituting (13) into (12), the error dynamics can be written as:

$$\dot{\tilde{\mathbf{x}}} = \left(\mathbf{A}_0 + \bar{\mathbf{L}}\mathbf{C}\right)\tilde{\mathbf{x}} + \mathbf{L}\tilde{\mathbf{v}} + \tilde{\mathbf{u}}, \tag{14}$$

where $\mathbf{A}_0 = \begin{bmatrix} \mathbf{0}_{2\times2} & \mathbf{M} \\ \mathbf{0}_{3\times2} & \mathbf{N} \end{bmatrix}$ with $\mathbf{M} = \begin{bmatrix} 0 & -\omega_2 & 0 \\ 0 & \omega_1 & 0 \end{bmatrix}$ and $\mathbf{N} = \begin{bmatrix} 0 & 0 & 0 \\ \alpha & -\alpha & 0 \\ 1 & 0 & 0 \end{bmatrix}$. Notice that while $\mathbf{N}$ is time-invariant, $\mathbf{M}$ is time-varying due to the appearance of ω_1 and ω_2. Furthermore, $\mathbf{A}_0$ is upper-block triangular. Denoting the ith element of $\tilde{\mathbf{x}}$ by $\tilde{x}_i$, it can be seen that in the part of error dynamics contributed by $\mathbf{A}_0$, $\tilde{x}_3, \tilde{x}_4$and $\tilde{x}_5$ can influence the dynamics of $\tilde{x}_1$and $\tilde{x}_2$ but not vice versa. To exploit the structural property of $\mathbf{A}_0$, the $\mathbf{C}$ matrix is restructured as $\mathbf{C} = \begin{bmatrix} \mathbf{I}_{2\times2} & \mathbf{0}_{2\times3} \\ \mathbf{0}_{2\times2} & \mathbf{R} \end{bmatrix}$ with $\mathbf{R} = \begin{bmatrix} 1 & -1 & 0 \\ 0 & 0 & 1 \end{bmatrix}$, and $\bar{\mathbf{L}}$ is chosen as a block diagonal matrix, or $\bar{\mathbf{L}} = \begin{bmatrix} \bar{\mathbf{L}}_a & \mathbf{0}_{2\times2} \\ \mathbf{0}_{3\times2} & \bar{\mathbf{L}}_b \end{bmatrix}$ where $\bar{\mathbf{L}}_a \in R^{2\times2}$and $\bar{\mathbf{L}}_b \in R^{3\times2}$ are sub-observer-gain matrices to be designed. The autonomous part of the error dynamics (i.e. $\tilde{\mathbf{v}} = \mathbf{0}$, $\tilde{\mathbf{u}} = 0$) can be written as by

$$\begin{aligned} \dot{\tilde{\mathbf{x}}} &= \left(\mathbf{A_0} + \bar{\mathbf{L}}\mathbf{C}\right)\tilde{\mathbf{x}} \\ &= \begin{bmatrix} \bar{\mathbf{L}}_a & \mathbf{M} \\ \mathbf{0}_{3\times2} & \mathbf{N} + \bar{\mathbf{L}}_b\mathbf{R} \end{bmatrix}\tilde{\mathbf{x}}. \end{aligned} \tag{15}$$

Although the autonomous system is time-varying, it is possible to choose appropriate $\bar{\mathbf{L}}_a$ and $\bar{\mathbf{L}}_b$ to achieve exponential stability if the elements of $\mathbf{M}$ (i.e. ω_1 and ω_2) are bounded. The reasoning is the following: The upper-block triangular structure retained in the system matrix makes the dynamics of $\tilde{x}_3, \tilde{x}_4$ and $\tilde{x}_5$ self-inclusive. Since the matrix-pair $(\mathbf{N}, \mathbf{R})$ is observable, one can make $\tilde{x}_3, \tilde{x}_4$and $\tilde{x}_5$ exponentially stable by simply choosing an $\bar{\mathbf{L}}_b$ matrix to place the poles of $\mathbf{N} + \bar{\mathbf{L}}_b\mathbf{R}$ in the left half plane. On the other hand, if $\bar{\mathbf{L}}_a$ is chosen to be Hurwitz, then $\tilde{x}_1$ and $\tilde{x}$ can be viewed as the outputs of a linear, stable filter $((sI - \bar{\mathbf{L}}_a)^{-1})$ whose inputs $\mathbf{M}\begin{bmatrix} \tilde{x}_3 \\ \tilde{x}_4 \\ \tilde{x}_5 \end{bmatrix} = \begin{bmatrix} -\omega_2\tilde{x}_4 \\ \omega_1\tilde{x}_4 \end{bmatrix}$ are bounded by exponentially converging signals ($|\omega_2|_{\max}|\tilde{x}_4|$ and $|\omega_1|_{\max}|\tilde{x}_4|$). Therefore the two error state variables are also exponentially stable.

The actual error dynamics in (14) contains $\tilde{\mathbf{v}}$ and $\tilde{\mathbf{u}}$ acting as perturbed inputs to the autonomous system. The influence of $\tilde{\mathbf{v}}$ and $\tilde{\mathbf{u}}$ on the error convergence can be kept small by constructing an appropriate estimations $\hat{\mathbf{v}}$ and $\hat{\mathbf{u}}$ to cancel $\mathbf{v}$ and $\mathbf{u}$ respectively. As for cancelling $\mathbf{v}$, the a_{hpf} signal contained in its Z_s-axis component, is left intact. This is because a_{hpf} is intentionally made to be a high-frequency signal with cut-off at α. It will be automatically filtered out by the observer dynamics if the observer poles are slower than α. Therefore, Constructing $\hat{\mathbf{v}}$ only requires the estimation of centrifugal acceleration. On the other hand, constructing $\hat{\mathbf{u}}$ only requires the estimation of a_{cz}, which is the Z_s-axis component of the centrifugal acceleration.

A. Estimation of centrifugal acceleration

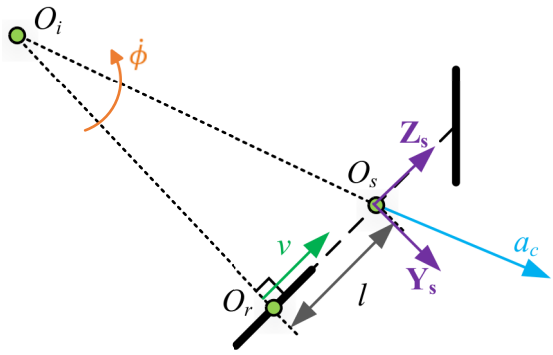

Fig. 3. Simplified 2-D bicycle model

In the simplified 2-D bicycle model shown in Fig. 3, O_s is the origin of the sensor frame $X_sY_sZ_s$, O_r is the center of the rear wheel, O_i is the instantaneous center of rotation, and $\ell = \overline{O_sO_r}$. The direction of rear wheel' velocity ($\overrightarrow{v}$) is aligned with $\overline{O_rO_s}$ but perpendicular to $\overline{O_iO_r}$. Given the yaw rate $\dot{\phi}$ and the rear wheel speed v, the turning radius of the rear wheel $\overline{O_iO_r} = v/\dot{\phi}$. Because $\triangle O_iO_rO_s$ is now a rectangular triangle, $\overline{O_iO_s}$, which is the turning radius of the bicycle at O_s, is equal to $\sqrt{\ell^2 + (\frac{v}{\dot{\phi}})^2}$. The centrifugal acceleration has a magnitude of $a_c = \overline{O_iO_s}\cdot\dot{\phi}^2 = \dot{\phi}\sqrt{\ell^2\dot{\phi}^2 + v^2}$ and its direction is along $\overrightarrow{O_iO_s}$. One can thus obtain the vectorial decomposition of the centrifugal acceleration components along the three sensor axes as

$$\begin{bmatrix} a_{cx} \\ a_{cy} \\ a_{cz} \end{bmatrix} = \begin{bmatrix} 0 \\ v\dot{\phi} \\ \ell\dot{\phi}^2 \end{bmatrix}.$$

While v is directly measurable, the computation of $\dot{\phi}$ is based on the trigonometrical relationship between the first

and second components of $\boldsymbol{\omega}$ in (3), or

$$\dot{\phi} = \frac{\omega_1 c_\theta - \omega_2 s_\theta}{c_\psi}. \tag{16}$$

When both ψ and θ are small, $c_\theta \approx c_\psi \approx 1$ and $s_\theta \approx 0$. The yaw rate in (16) can be approximated by ω_1, so the centrifugal acceleration can be estimated as

$$\begin{bmatrix} \hat{a}_{cx} \\ \hat{a}_{cy} \\ \hat{a}_{cz} \end{bmatrix} = \begin{bmatrix} 0 \\ v\omega_1 \\ \ell\omega_1^2 \end{bmatrix},$$

where $\hat{a}_{c(\bullet)}$ is the estimation for $a_{c(\bullet)}$.

V. Experimental Validation

A prototype bicycle which uses $500W$ brushless DC wheel motor as the rear wheel is constructed for experimental validation. The motor torque is regulated by controlling the motor current via a motor driver. The IMU sensor used is LSM9DS0 manufactured by SparkFun Electronics[8]. The sensor contains a three-axis accelerometer, a three-axis gyroscope, and a three-axis magnetometer. The measurements from the magnometer are not used in sensor fusion because their susceptibility to electromagnetic interference from the power electronics[1]. Both the motor control and sensor fusion algorithms are implemented on Microchip's dsPIC30F4011 micro-controllers[9]. The photo of the prototype bicycle is shown in Fig. 4.

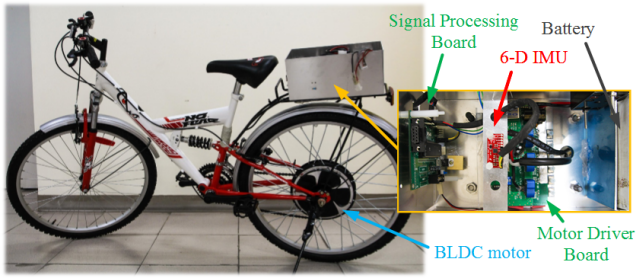

Fig. 4. Photo of the power-assist electric bicycle

In the sensor fusion algorithm, the filter bandwidth α is set to $1\ rad/s$. The poles of the observer, or the eigenvalues of $\bar{\mathbf{L}}_a$ and $\mathbf{N} + \bar{\mathbf{L}}_b\mathbf{R}$ assume Butterworth pattern with radius of $1\ rad/s$. This provides a good balance between the filtering of the high-frequency sensor noise and state estimates convergence. In the power-assist compensation on the prototype bicycle, since the third state of $\mathbf{x}$ is equal to $-gs_\phi$, the gravity compensation and friction compensation can be respectively computed by $-M\hat{x}_3$ and $f_r M\sqrt{g^2 - \hat{x}_3^2}$ where $\hat{x}_3$ is the third element of $\hat{\mathbf{x}}$. Particularly, the friction coefficient f_r is chosen to be 0.015 based on the road testing data. Notice that to accommodate for estimation error and avoid over-compensation, the mass M used for gravity and friction compensations is only 90% of the total mass.

As for mass compensation, $\eta = 0.244$ is adopted. Such a ratio corresponds to about 90% of its maximum value ($\frac{m_b}{M}$). The longitudinal acceleration is approximated by

$$a \approx \hat{g}_{s3} - a_{s3} + \hat{a}_{cz} = \hat{x}_3 - a_{s3} + \ell\omega_1^2. \tag{17}$$

where $\hat{g}_{s3}$ is the estimation for g_{s3} and by definition is equal to $\hat{x}_3$.

A road riding test was conducted on the E-bike to verify the performance of the proposed sensor fusion algorithm and power-assist function. During the test, the rider first pedaled to accelerate the bicycle on the level ground, then made two right turns, finally climbed uphill. This test was repeated without power assist for comparison purposes. The velocity v, estimations of the roll and pitch (θ, ψ) angles , yaw rate given by (16), estimated acceleration in (17), and the EMG signal of the quadriceps muscle for each of the two tests are shown in Fig. 5. With similar maneuvering for the two tests, the power-assist function reduces the RMS magnitude of the EMG signal from $0.617volts$ to $0.49volts$. This verifies the validity of the sensor fusion algorithm and power-assist function.

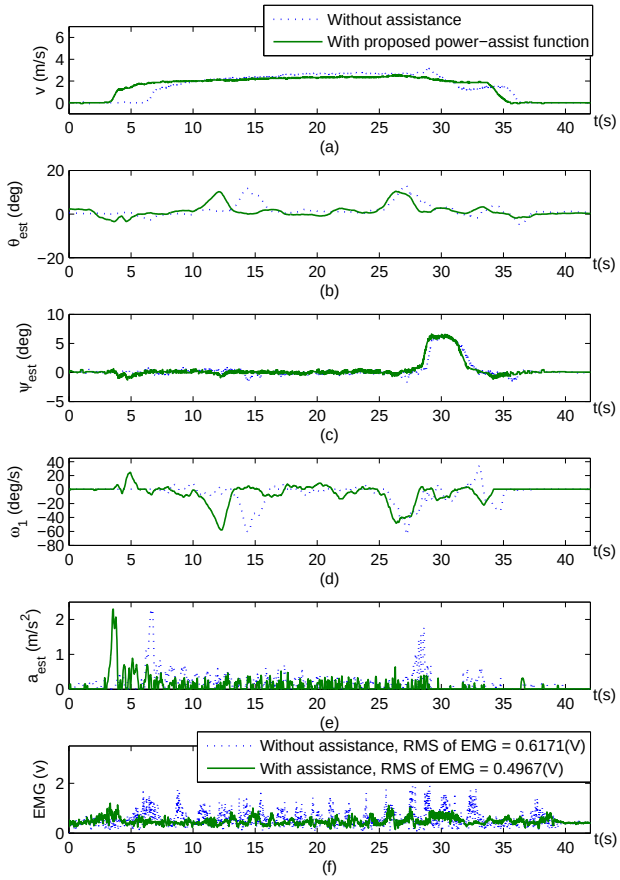

Fig. 5. Comparisons between the power-assist bike and non-power-assist bike in a road-riding test

[1]However, one may find the magnetometer particularly useful when determination of the absolute orientation (ϕ) of the bicycle is needed.

VI. Conclusions

This paper is devoted to developing a sensor fusion algorithm for electric bicycles. With the algorithm, one can replace the expensive, bulky torque sensors by low-cost, compact IMU sensors and wheel encoders to achieve power-assist function. The sensor fusion algorithm is observer-based. A systematic procedure to construct the observer is provided. Although the observer model is time-varying and is fifth-dimensional, by exploiting the model structure, the convergence of the estimation errors can be guaranteed by properly choosing two low-dimensional constant gain matrices. The performance of the sensor fusion algorithm and the power-assist function is validated via a road test. With power assist, the magnitude of the rider's EMG signal is significantly reduced compared to the pure manual pedaling case. The results in this study can be directly applied to power assist other manual-driven vehicles such as wheelchairs.

APPENDIX

The constraint on the assistive ratio η is due to the fact that the rider is not rigidly connected to the bicycle. In Fig. 6, the coupling between the rider and the bicycle is modeled by a parallel combination of a spring k and a damper b. In this figure, other than the bicycle's mass m_b, the rider's mass is represented by m_r, so the total mass $M = m_b + m_r$. Furthermore, x_b and x_r respectively denote the absolute displacements of the bicycle and the rider, and F_m is the propulsion force generated by the motor.

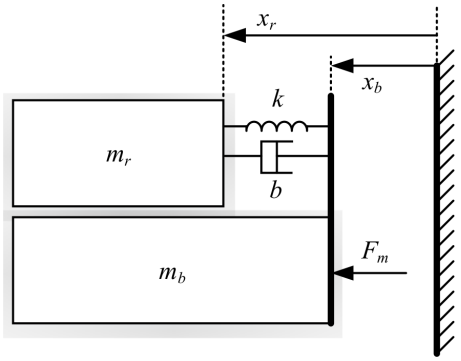

Fig. 6. Schematic of the modified bicycle model with two lumped masses and spring-damper connection

The equations of motion for the rider and the bicycle are respectively given by

$$m_r\ddot{x}_r = -k(x_r - x_b) - b(\dot{x}_r - \dot{x}_b), \tag{18}$$

$$m_b\ddot{x}_b = -k(x_b - x_r) - b(\dot{x}_b - \dot{x}_r) + F_m. \tag{19}$$

Because friction compensation and gravity compensation do not affect the stability, for analysis purposes, only mass compensation is considered:

$$F_m = \eta M\ddot{x}_b. \tag{20}$$

Substituting (20) into (19) and then taking Laplace transforms on the resultant equation and (18) allow one to compute the characteristic equation $\Delta(s)$ as

$$\Delta(s) = s^2\{s^2 + \frac{M(1-\eta)b}{m_r(m_b - \eta M)}s + \frac{M(1-\eta)k}{m_r(m_b - \eta M)}\} = 0.$$

In addition to the two rigid body modes, the condition for the other two poles to be in the left half plane is to have $m_b - \eta M > 0$.

ACKNOWLEDGMENT

The authors gratefully acknowledge the support provided by Ministry of Science and Techonlogy in Taiwan.

References

[1] Marien van Ditten, *Torque Sensing for E-Bike Applications*, Master Thesis, Department of Precision and Microsystems Engineering, Delft University of Technology, June 27, 2011

[2] T. Kurosawa, Y. Fujimoto, and T. Tokumaru, "Estimation of Pedaling torque for electric power assisted bicycles, " In Proceedings of the 40th Annual Conference of the IEEE Industrial Electronics Society, pp. 2756-2761, 2014.

[3] H. Kawajiri, et. al., "Sensorles Pedaling Torque Estimation by Front and Rear Wheels Independently Driven Power Assist Bicycle," IEEE International Conference on Mechatronics, Mar. 6-8, 2015, pp. 364-369.

[4] J. Gross, el. al, "Flight Test Evaluation of Sensor Fusion Algorithms for Attitude Estimation". IEEE Transactions on Aerospace and Electronic Systems 48 (3): 2128–2139, July, 2012.f

[5] J. L. Crassidis, and F. L. Markley, "Unscented Filtering for Spacecraft Attitude Estimation" Journal of Guidance Control and Dynamics, July, 2003.

[6] D. Bevly, J. Ryu, and J. Gerdes, "Integrating INS sensors with GPS Measurements for Continuous Estimation of Vehicle Sideslip, roll and tire Corning Stiffness, " IEEE Transactions on Intelligent Transportation Systems, vol. 7, pp. 483-493, Dec. 2006.

[7] S. Antonov, A. Fehn, and A. Kugi, "Unscented Kalman Filter for Vehicle State Estimation, " Vehicle System Dynamics, pp. 1497-1520, 2009.

[8] https://www.sparkfun.com/products/retired/12636

[9] http://www.microchip.com/wwwproducts/Devices.aspx?product=dsPIC30F4011